⌘ *Author's Choice*

Visualization of Structural Changes Accompanying Activation of *N*-Methyl-D-aspartate (NMDA) Receptors Using Fast-scan Atomic Force Microscopy Imaging*

Yuki Suzuki[‡1], **Tom A. Goetze**[§], **David Stroebel**[¶], **Dilshan Balasuriya**[§2], **Shige H. Yoshimura**[‡], **Robert M. Henderson**[§], **Pierre Paoletti**[¶], **Kunio Takeyasu**[‡3], and **J. Michael Edwardson**[§4]

From the [‡]Laboratory of Plasma Membrane and Nuclear Signaling, Graduate School of Biostudies, Kyoto University, Kyoto 606-8501, Japan, the [§]Department of Pharmacology, University of Cambridge, Cambridge CB2 1PD, United Kingdom, and the [¶]École Normale Supérieure, Institut de Biologie de l'École Normale Supérieure (IBENS), CNRS UMR 8197, INSERM U1024, 75005 Paris, France

Background: NMDA receptors mediate fast excitatory synaptic transmission.
Results: NMDA receptors in lipid bilayers were imaged during activation using fast-scan atomic force microscopy.
Conclusion: The height of the receptor fell rapidly by ~1 nm upon activation.
Significance: Our study provides a glimpse into the behavior of individual NMDA receptors under near-physiological conditions.

NMDA receptors are widely expressed in the central nervous system and play a major role in excitatory synaptic transmission and plasticity. Here, we used atomic force microscopy (AFM) imaging to visualize activation-induced structural changes in the GluN1/GluN2A NMDA receptor reconstituted into a lipid bilayer. In the absence of agonist, AFM imaging revealed two populations of particles with heights above the bilayer surface of 8.6 and 3.4 nm. The taller, but not the shorter, particles could be specifically decorated by an anti-GluN1 antibody, which recognizes the S2 segment of the agonist-binding domain, indicating that the two populations represent the extracellular and intracellular regions of the receptor, respectively. In the presence of glycine and glutamate, there was a reduction in the height of the extracellular region to 7.3 nm. In contrast, the height of the intracellular domain was unaffected. Fast-scan AFM imaging combined with UV photolysis of caged glutamate permitted the detection of a rapid reduction in the height of individual NMDA receptors. The reduction in height did not occur in the absence of the co-agonist glycine or in the presence of the selective NMDA receptor antagonist D(−)-2-amino-5-phosphonopentanoic acid, indicating that the observed structural change was caused by receptor activation. These results represent the first demonstration of an activation-induced effect on the structure of
the NMDA receptor at the single-molecule level. A change in receptor size following activation could have important functional implications, in particular by affecting interactions between the NMDA receptor and its extracellular synaptic partners.

Ionotropic glutamate receptors (iGluRs)[5] mediate fast synaptic transmission in the central nervous system. The iGluRs can be classified into AMPA, kainate, and NMDA receptor subfamilies (1, 2), and all three subfamilies assemble as tetrameric complexes of four homologous pore-forming subunits. The various subunits share a common modular architecture, consisting of a large extracellular N-terminal domain (NTD), an agonist-binding domain (ABD), a transmembrane domain, and an intracellular C-terminal domain (1, 2). The x-ray crystal structure of a homomeric GluA2 AMPA receptor (3) revealed that the receptor assembles as a large Y-shaped structure, protruding from the membrane by ~14 nm, with the NTDs, ABDs, and transmembrane domains arranged in layers. As expected from studies on isolated domains (4, 5), the NTDs and ABDs both assemble as dimers of dimers but with few contacts between the two constitutive dimers. The agonist-binding sites are located within clamshell-like structures that constitute the ABDs, and binding of agonists results in closure of the clamshells. This movement is likely transmitted to the M3 transmembrane helices, resulting in opening of the ion channel (3).

NMDA receptors are key players in the development of synaptic plasticity and consequent higher functions, including learning and memory, and NMDA receptor dysfunction has been implicated in various neurological disorders such as chronic pain, Alzheimer disease, and schizophrenia (6). Hence, the NMDA receptor also represents a significant therapeutic target. NMDA receptors are obligate heterotetramers contain-

---

[1] Japan Society for the Promotion of Science Research Fellow.
[2] Recipient of a David James Bursary from the Department of Pharmacology, University of Cambridge.
[3] To whom correspondence may be addressed. Tel. and Fax: 81-75-753-6852; E-mail: takeyasu@lif.kyoto-u.ac.jp.
[4] To whom correspondence may be addressed. Tel.: 44-1223-334014; Fax: 44-1223-334100; E-mail: jme1000@cam.ac.uk.

ing three basic types of subunit: GluN1, GluN2, and GluN3 (1, 2, 7).

NMDA receptors likely adopt a general arrangement similar to that of AMPA receptors (1, 2, 8). Crystallographic and functional studies have shown that within a GluN1/GluN2 receptor, the NTDs and ABDs assemble as local heterodimers (8–12). As with AMPA receptors, upon agonist binding, the two neighboring ABDs are thought to swing apart, leading to channel opening (2, 8). However, a direct demonstration of these conformational changes in the context of the intact receptor is lacking. In this study, we used atomic force microscopy (AFM) to monitor the effect of receptor activation on the structure of individual GluN1/GluN2A NMDA receptors reconstituted in a lipid bilayer with nanometer resolution. Using fast-scan AFM, we show that photolytic release of glutamate into a glycine-containing buffer causes a rapid decrease in the height of the extracellular region of the receptor. To our knowledge, our results represent the first visualization of activation-induced structural changes in the NMDA receptor at the single-molecule level.

EXPERIMENTAL PROCEDURES

NMDA Receptor Subunit Constructs—The pcDNA3-based expression plasmids for rat GluN1-1a and rat GluN2A have been described previously (13). A FLAG/His$_8$ epitope tag was introduced between residues 851 and 852 of GluN2A, *i.e.* 15 residues downstream of the final transmembrane segment (*i.e.* …CFTG^{851}DYKDDDDKHHHHHHHHV^{852}CSD . . . , with the tag underlined).

Assessment of the Functional Activity of the Subunit Constructs—Recombinant NMDA receptors were expressed in *Xenopus laevis* oocytes after nuclear co-injection of 30 nl of a mixture of cDNAs (10 ng/μl, 1:1 ratio) coding for wild-type rat GluN1-1a and either wild-type or FLAG/His$_8$-tagged rat GluN2A. Oocytes were prepared, injected, voltage-clamped, and superfused as described previously (14). The heavy metal chelator diethylenetriaminepentaacetic acid (10 μM) was added to all bathing solutions to avoid tonic inhibition of GluN2A-containing NMDA receptors by contaminant zinc (14). Data were collected and analyzed using pCLAMP 9.2 (Molecular Devices) and fitted using KaleidaGraph (Synergy Software). All recordings were performed at a holding potential of −60 mV and at room temperature.

Expression and Purification of NMDA Receptors—NMDA receptors were expressed in HEK293T (tsA201) cells. Cells were grown in Dulbecco's modified Eagle's medium (Sigma) supplemented with 10% (v/v) fetal bovine serum, 100 units/ml penicillin, and 100 μg/ml streptomycin in an atmosphere of 5% CO$_2$/air. Transfection was carried out using either Effectene transfection reagent (Qiagen) or calcium phosphate precipitation. After transfection, cells were incubated for 24–48 h at 37 °C to allow expression of receptors.

All purification steps were carried out at 4 °C. For receptors to be imaged in air, transfected cells were solubilized in 1% Triton X-100 for 1 h before centrifugation at 61,740 × g to remove insoluble material. Solubilized protein was incubated with anti-FLAG-agarose beads for 3 h. NMDA receptors containing FLAG-tagged GluN2A were eluted with 3×FLAG peptide (0.15 mg/ml).

For receptors to be integrated into bilayers, a crude membrane fraction prepared from transfected cells was solubilized in 40 mM *n*-dodecyl-β-D-maltoside for 1 h. The extract was centrifuged at 60,000 × g to remove insoluble material, and the supernatant was incubated with Ni^{2+}-agarose beads (ProBond, Invitrogen) for 30 min. The beads were washed, and the bound protein was eluted with increasing concentrations of imidazole (2× 80, 2× 160, and 2× 400 mM; 0.5-ml fractions). The eluted protein sample (usually the second 80 mM and both 160 mM fractions) was concentrated 10-fold using a centrifugal filter (Amicon) and then incubated with anti-FLAG-agarose beads, followed by elution with 3×FLAG peptide as described above. The sample was diluted 5-fold with 1% CHAPS and then concentrated using an Amicon filter. Purified proteins were analyzed by SDS-PAGE and immunoblotting using mouse anti-GluN1 monoclonal antibody (clone 54.1, MAB363, Millipore) and rabbit anti-GluN2A monoclonal antibody (A12W, 04-901, Millipore).

Integration of NMDA Receptors into Liposomes—Chloroform solutions of 1,2-dioleoyl-*sn*-glycero-3-phosphatidylcholine and brain l-α-phosphatidylserine (Avanti Polar Lipids) were mixed at a molar ratio of 3:1. The chloroform was then evaporated under a stream of nitrogen gas, and the lipids were redissolved in HEPES-buffered saline (100 mM NaCl and 50 mM HEPES-NaOH, pH 7.6) containing 1% CHAPS at a concentration of 2 mg/ml. Solubilized lipid (100 μl, 200 μg) was mixed with 0.5–1 μg of purified NMDA receptor (100 μl) and then dialyzed against detergent-free HEPES-buffered saline at room temperature for 3 days. The dialyzed sample was used for AFM imaging directly or after incubation for 12 h at 4 °C with anti-GluN1 or anti-HA (control) monoclonal antibody.

AFM Imaging in Air—Isolated receptors were imaged either alone or following overnight incubation at 4 °C with a 1:2 molar ratio (~0.2 nM protein concentration) of anti-GluN1 antibody. Proteins were diluted to a final concentration of 0.04 nM, and 45 μl of the sample was allowed to adsorb to freshly cleaved mica disks. After a 5-min incubation, the sample was washed with Biotechnology Performance Certified water (Sigma) and dried under nitrogen. Imaging was performed with a Veeco Digital Instruments multimode atomic force microscope controlled by a NanoScope IIIa controller. Samples were imaged in air using tapping mode. The silicon cantilevers used had a drive frequency of ~300 kHz and a specified spring constant of 40 newtons/m (Olympus, Tokyo, Japan). The applied imaging force was kept as low as possible ($A_s/A_0 \sim 0.85$).

AFM Imaging under Fluid—The fast-scan AFM system (15) has been described previously (16). In this study, a newly developed piezo scanner with resonant frequencies of 30 kHz (*xy*) and 600 kHz (*z*) was introduced. Silicon nitride cantilevers (BL-AC7EGS-A2, Olympus) with a resonant frequency of 600–1000 kHz in water and a spring constant of 0.1–0.2 newtons/m were used. A sharp probe was deposited on each cantilever by electron beam deposition using a Nanotools device. A typical free oscillation amplitude was 4 nm, and the amplitude set point during scanning was ~70% of this value.

A droplet (3 μl) of proteoliposome suspension was deposited on the surface of a freshly cleaved mica disk (diameter, 1 mm). After incubation for 30 min at room temperature, the mica
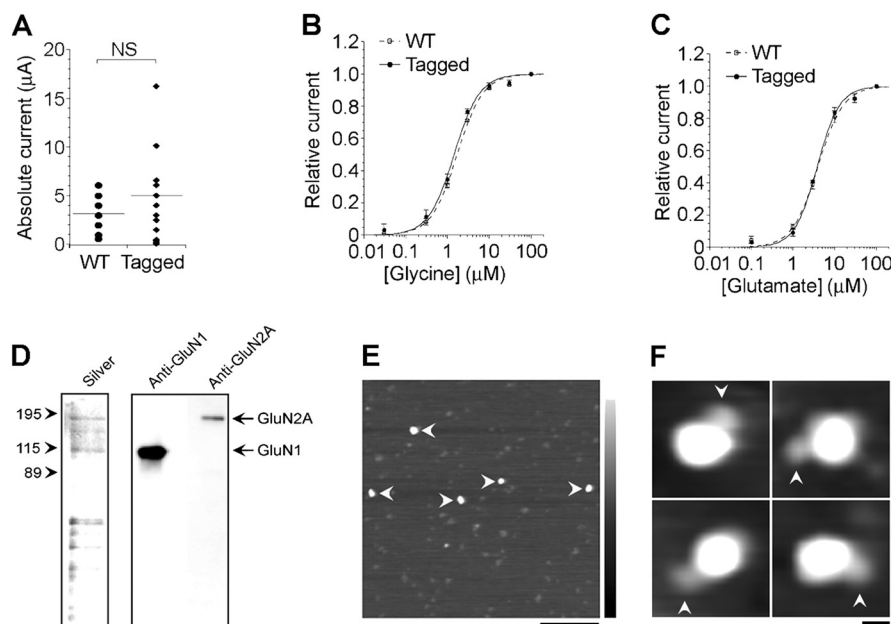
FIGURE 1. **Expression, isolation, and analysis of NMDA receptors.** *A–C*, functional properties of wild-type and FLAG/His$_8$-tagged GluN2A coexpressed with untagged GluN1 in *Xenopus* oocytes. *A*, currents activated by saturating concentrations of L-glutamate and glycine (100 μM for both) in *Xenopus* oocytes expressing untagged GluN1 in combination with either wild-type (●; $n = 9$) or tagged (♦; $n = 16$) GluN2. The *horizontal lines* denote the means of the two distributions, which are not significantly (*NS*) different from each other ($p = 0.174$, Student's *t* test). *B*, glycine concentration-response curves in the presence of 100 μM glutamate. Curves were fitted with the Hill equation. EC$_{50}$ values were 1.7 ± 0.1 and 1.4 ± 0.1 μM for wild-type and tagged GluN2A, respectively. Hill coefficients (n_H) were 1.4 ± 0.1 and 1.4 ± 0.1 for wild-type and tagged GluN2A, respectively ($n = 3–4$). *C*, glutamate concentration-response curves in the presence of 100 μM glycine. EC$_{50}$ values were 3.9 ± 0.2 and 3.8 ± 0.2 μM for wild-type and tagged GluN2A, respectively. n_H values were 1.4 ± 0.1 and 1.6 ± 0.1 for wild-type and tagged GluN2A, respectively ($n = 3–4$). *D*, samples of protein isolated from cotransfected HEK293T cells by affinity chromatography were analyzed by SDS-PAGE, followed by either silver staining (*left panel*) or immunoblotting using anti-GluN1 and anti-GluN2A antibodies (*right panel*). *E*, low-magnification AFM image of a sample of isolated NMDA receptors (*arrowheads*). *Scale bar* = 200 nm; *shade-height scale* = 0–5 nm. *F*, gallery of zoomed images of NMDA receptor particles that were decorated with an anti-GluN1 antibody (*arrowheads*). *Scale bar* = 20 nm; *shade-height scale* = 0–5 nm.

surface was gently washed several times with HEPES-buffered saline to remove unadsorbed proteoliposomes. AFM imaging in tapping mode was performed in the same buffer solution. To photolyze caged glutamate (4-methoxy-7-nitroindolinyl-L-glutamate; Tocris) on the sample stage, UV light (330–385 nm) was directed through the objective lens. Adhesion of the bilayer to the mica support was sufficient to minimize random diffusion of NMDA receptors. (The average two-dimensional diffusion coefficient was 0.5 ± 0.3 nm²·s⁻¹ (mean ± S.D.).) AFM images were obtained with a scanning speed of one frame/s. Where appropriate, vertical sections were taken in each frame through the highest point of the receptor.

Volume Measurements—Particle heights and radii were measured manually and used to calculate molecular volumes according to Equation 1,

$$V_m = (\pi h/6)(3r^2 + h^2) \qquad \text{(Eq. 1)}$$

where h is the maximal particle height and r is the radius, taken at half the height to minimize tip convolution (17). This equation assumes that the particle image has the form of a spherical cap.

The theoretical volume of the extracellular region of an intact NMDA receptor tetramer was estimated assuming that it has an overall structure similar to that of the AMPA receptor (3). After removal of the transmembrane domains (amino acids 523–620 and 790–817 of each subunit) from the AMPA receptor crystal structure (Protein Data Bank code 3KG2) using Swiss-PdbViewer (version 4.1), a volume of 369 nm³ was calcu-

lated. This volume, which includes enclosed cavities, is based on the space-filling/Corey-Pauling-Koltun model with a fixed radius for each atom. The structure was smoothed with a probe size of 1.4 Å.

To determine the degree of overestimation of particle volumes as a result of convolution caused by the geometry of the scanning tip, gold particles of known diameter (and hence volume) were imaged under the same conditions as used for the proteolipid bilayers. For this purpose, a droplet (3 μl) of gold colloid (diameter, 5 nm; BB International, Cardiff, United Kingdom) was deposited on the surface of a freshly cleaved mica disk.

RESULTS

To allow us to isolate NMDA receptors, we added a FLAG/His$_8$ epitope tag downstream of the final transmembrane segment of GluN2A. The functional activity of this construct was checked by coexpression with wild-type GluN1 in *X. laevis* oocytes. Robust currents, not significantly different from wild type, were recorded with the tagged GluN2A construct (Fig. 1*A*). Furthermore, the presence of the tag did not significantly affect the sensitivity of the receptor (EC$_{50}$) to either glycine (Fig. 1*B*) or glutamate (Fig. 1*C*). Hence, NMDA receptors containing tagged GluN2A are efficiently delivered to the oocyte plasma membrane and function normally.

It is generally accepted that GluN1 subunits can form stable intracellular homomers, whereas GluN2 subunits cannot (18, 19). Heteromeric NMDA receptors were therefore isolated

from cotransfected HEK293T cells by affinity chromatography using the FLAG/His$_8$ tag on GluN2A. Analysis of the isolated sample on a silver-stained gel revealed the presence of major bands at 120 and 180 kDa (Fig. 1*D*, *left panel*). Immunoblotting using appropriate anti-subunit antibodies indicated that these two bands were GluN1 and GluN2A, respectively (Fig. 1*D*, *right panel*).

Isolated NMDA receptors were subjected to AFM imaging in air after adsorption onto mica supports. A typical low-magnification AFM image is shown in Fig. 1*E*. Several large particles of approximately equal sizes can be seen (*arrowheads*). The isolated protein was then incubated with the same anti-GluN1 antibody used for the immunoblots (see above), which recognizes the ABD, and again imaged by AFM. A substantial proportion (257/1140, 23%) of the large particles were now decorated by smaller particles (*arrowheads*), representing anti-GluN1 antibodies bound to NMDA receptors (Fig. 1*F*). These results demonstrate that although the receptor preparation is not completely pure, an NMDA receptor population can be reliably detected by AFM imaging.

Isolated NMDA receptors were next integrated into liposomes (3:1 phosphatidylcholine/l-α-phosphatidylserine), a process that will exclude any non-membrane proteins present in the isolated protein sample. The proteoliposomes were deposited onto a mica surface to produce a supported proteolipid bilayer. AFM imaging of this bilayer under fluid in the absence of agonists revealed a smooth layer of thickness 4.5 ± 0.4 nm (*n* = 52), as expected for a single bilayer (20), containing small particles (Fig. 2*A*). A section through one of the integrated particles revealed a height above the bilayer of 8.2 nm (Fig. 2*B*). Imaging of a number of these particles revealed two distinct height populations; for example, Fig. 2*C* shows two particles of with heights of 3.1 nm (*arrowhead*) and 8.2 nm (*arrow*). A frequency distribution of heights had two peaks at 3.4 ± 1.4 nm (mean ± S.D.) and 8.6 ± 0.9 nm (*n* = 41, where *n* is the total number of particles in the height distribution) (Fig. 2*D*). Given that the likely ratio of molecular masses on the intracellular and extracellular faces of the plasma membrane is ~1:2, assuming a GluN1/GluN2A stoichiometry of 2:2, we speculated that these two height populations represent the intracellular and extracellular domains of the receptor, respectively.

The volumes of the individual particles were calculated using Equation 1. As was seen for the distribution of heights, the frequency distribution of volumes had two peaks at 761 ± 535 and 2955 ± 392 nm^3 (*n* = 41) (Fig. 2*E*). Assuming that the NMDA receptor assembles in a manner similar to the AMPA receptor, the crystal structure of the AMPA receptor can be used to provide an estimate of the volume of the extracellular domain of the NMDA receptor. Analysis of the AMPA receptor crystal structure using Swiss-PdbViewer yielded a volume of 369 nm^3. Hence, the measured volume of the extracellular domain of the receptor is apparently overestimated by 8.0-fold by AFM imaging under fluid.

It is well known that measurement of molecular volumes by AFM is complicated by the convolution introduced by the geometry of the scanning tip (17) and that this problem is more severe for a taller particle. It is therefore to be expected that the volume of a receptor protruding 8–9 nm from a lipid bilayer
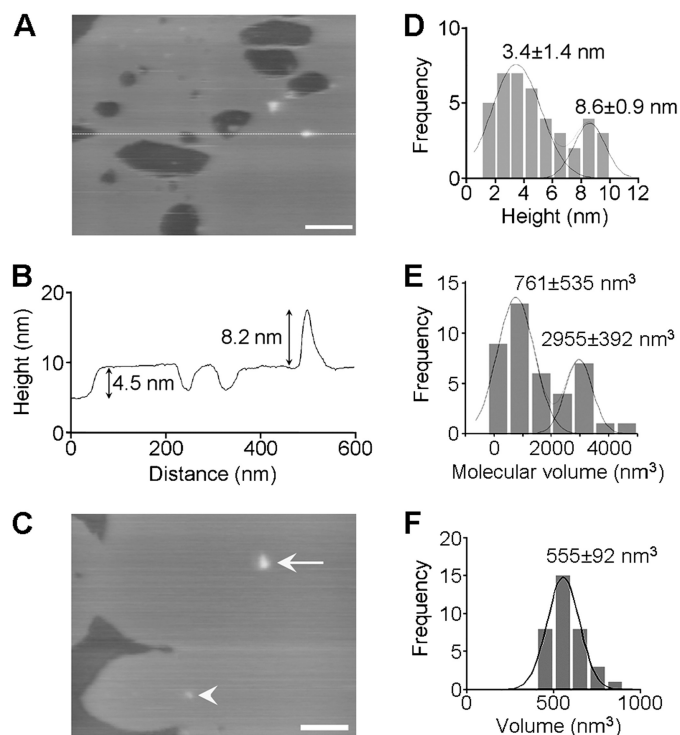

FIGURE 2. **AFM imaging of NMDA receptors integrated into supported lipid bilayers.** *A*, AFM image of a bilayer containing NMDA receptors. *Scale bar* = 100 nm; height range = 20 nm. *B*, section through the bilayer taken at the position indicated by the *line* in *A*. *C*, AFM image of a bilayer in the absence of agonists. The *arrowhead* indicates a particle with a height of 3.1 nm; the *arrow* indicates a particle with a height of 8.2 nm. *Scale bar* = 100 nm; height range = 20 nm. *D*, frequency distribution of heights of NMDA receptor particles (*n* = 41). Fitted Gaussian curves are overlaid on the histogram. *E*, frequency distribution of volumes of NMDA receptor particles (*n* = 41). Fitted Gaussian curves are overlaid on the histogram. *F*, frequency distribution of volumes of 5-nm gold particles (of true volume 65 nm^3) purchased from BB International (*n* = 35). A fitted Gaussian curve is overlaid on the histogram.

would be considerably overestimated. To determine the actual degree of overestimation, we imaged 5-nm gold particles under fluid and calculated their volumes based on the measured heights and radii. (Note that a spherical gold particle will also replicate the "overhang" found in the Y-shaped structure of the AMPA receptors and by analogy also in the NMDA receptor.) A frequency distribution of volumes of the gold particles is shown in Fig. 2*F*. The peak volume is 555 ± 92 nm^3 (*n* = 35), representing an 8.5-fold overestimation of the true volume (65 nm^3), similar to the degree of overestimation of the receptor particles. This analysis therefore indicates that the volume of the larger particle population is consistent with the volume of the extracellular domain of an intact tetrameric NMDA receptor.

To further characterize the two particle populations, we incubated the proteoliposomes with the antibody against the ABD of the GluN1 subunit that was described above. Fig. 3*A* shows an AFM image of a proteolipid bilayer that had been incubated with the antibody. Antibody-decorated particles are indicated by *arrowheads*. Fig. 3*B* shows a gallery of particles that were decorated by antibodies. No decorated particles were seen when a control antibody (anti-HA) was used. The frequency distribution of heights of the antibody-decorated particles (determined as illustrated in Fig. 3*C*) had a single peak at 8.3 ± 0.6 nm (*n* = 46) (Fig. 3*D*), demonstrating that the taller
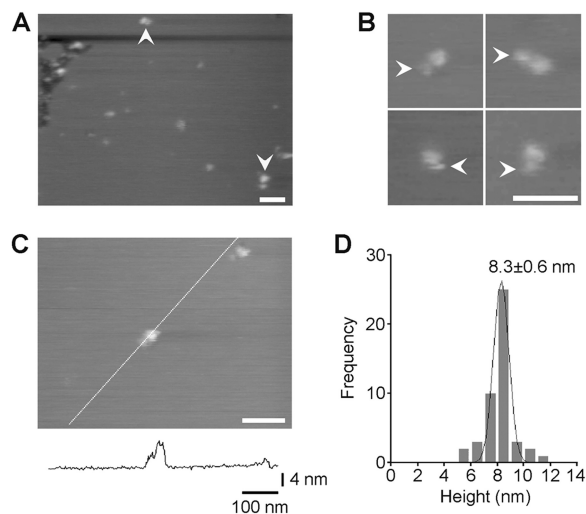
FIGURE 3. Antibody decoration of NMDA receptors integrated into lipid bilayers. *A*, AFM image of receptor-antibody complexes. Decorated NMDA receptors are indicated by the *arrowheads*. *Scale bar* = 100 nm; height range = 20 nm. *B*, zoomed images of receptors decorated by anti-GluN1 antibodies (*arrowheads*). *Scale bar* = 100 nm; height range = 20 nm. *C*, section through a receptor-antibody complex taken at the position indicated by the *line* in the image. *D*, frequency distribution of heights of decorated receptor particles ($n = 46$). A fitted Gaussian curve is overlaid on the histogram.

FIGURE 4. Effect of activation on the height of NMDA receptors. *A*, frequency distribution of heights of NMDA receptor particles in the presence of both 100 μM glycine and 100 μM glutamate ($n = 43$). *B*, frequency distribution of heights of NMDA receptor particles in the presence of 100 μM glutamate only ($n = 44$). *C* and *D*, frequency distributions of heights of NMDA receptor particles in the presence of both 100 μM glycine and 100 μM caged glutamate before (*C*; $n = 137$) and after (*D*; $n = 83$) UV irradiation. Fitted Gaussian curves are overlaid on the histograms.

particles do indeed represent the extracellular regions of the receptor. We therefore conclude that the two height peaks represent NMDA receptors that have become integrated into the bilayers either extracellular region down (the lower peak at 3.4 ± 1.4 nm) (Fig. 2*D*) or up (the higher peak at 8.6 ± 0.9 nm).

When bilayer-integrated GluN1/GluN2A NMDA receptors were incubated with saturating concentrations of agonists (100 μM glycine and 100 μM glutamate), the frequency distribution of the heights of the particles above the bilayer again showed two peaks at 3.5 ± 1.1 and 7.3 ± 0.9 nm ($n = 43$) (Fig. 4*A*). Significantly, the higher peak fell from 8.6 to 7.3 nm, whereas the lower peak did not change, indicating that the extracellular region, but not the intracellular region, undergoes a conformational change upon addition of the two agonists. In contrast, the frequency distribution of heights obtained after incubation of receptor-containing bilayers with 100 μM glutamate only (Fig. 4*B*) had peaks at 3.3 ± 1.0 and 8.4 ± 0.5 nm ($n = 44$), similar to the distribution for untreated receptors (Fig. 2*D*). Hence, both glycine and glutamate are required to produce the observed conformational change.

To control the activation of the NMDA receptor more precisely, the supported lipid bilayers were incubated in a solution containing glycine and caged glutamate (4-methoxy-7-nitroindolinyl-L-glutamate), and the glutamate was uncaged by UV photolysis. A frequency distribution of heights before uncaging showed the now-familiar two peaks at 3.4 ± 0.9 and 8.5 ± 0.6 nm ($n = 137$) (Fig. 4*C*). After uncaging, the two height peaks were at 3.8 ± 1.1 and 7.2 ± 0.7 nm ($n = 83$) (Fig. 4*D*). Hence, UV photolysis of glutamate caused a reduction in the higher peak similar to that caused by bath addition of glutamate, without significantly affecting the lower peak.

To monitor the time dependence of activation-induced changes in the heights of individual NMDA receptors, we turned to fast-scan AFM. Individual particles were identified,
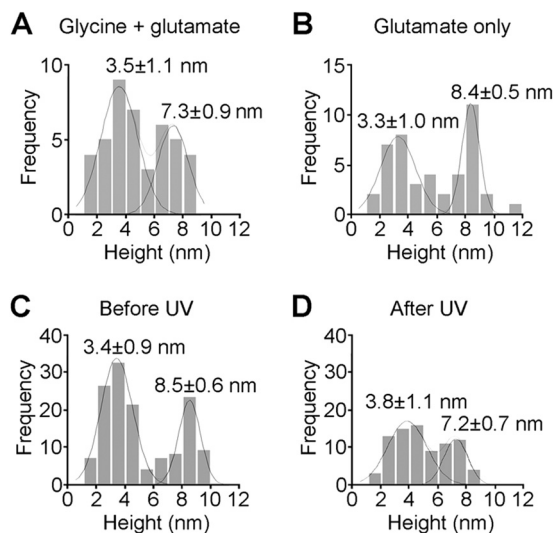
and glutamate was uncaged by UV photolysis while the particle was imaged repetitively. A representative particle before and after glutamate uncaging is shown in Fig. 5*A*. Before photolysis, the height of the receptor was 8.2 nm, whereas after photolysis, the height fell to 7.2 nm. Note that the bilayer has rearranged slightly in the interval (7 s) between the two images. When a particle was subjected to sequential imaging at a rate of one frame/s, the height of the particle above the bilayer before photolysis was 8.2 ± 0.3 nm (106 frames) (Fig. 5*B*); after photolysis, the height fell to 7.2 ± 0.4 nm (92 frames). The height of the particle fell rapidly (within 1 s) after UV photolysis but then fluctuated for several seconds before leveling out. Note that the thickness of the supported lipid bilayer was unaffected by uncaging of the glutamate: 4.4 ± 0.5 nm (57 frames) before and 4.3 ± 0.5 nm (49 frames) after uncaging. When glutamate uncaging was performed in the absence of glycine (Fig. 5*C*), the receptor did not show a significant reduction in height in response to photolysis: the heights before and after photolysis were 8.0 ± 0.3 nm (74 frames) and 7.9 ± 0.4 nm (100 frames), respectively. These results demonstrate that glycine is required for the conformational change in the extracellular domain of the receptor. Finally, we tested the effect of the competitive NMDA receptor antagonist D($-$)-2-amino-5-phosphonopentanoic acid (100 μM). Now, even when glutamate (100 μM) was uncaged in the presence of glycine (100 μM), the height of the receptor remained unchanged: 8.3 ± 0.3 nm (18 frames) before and 8.3 ± 0.2 nm (151 frames) after uncaging (Fig. 5*D*).

The mean particle heights before and after uncaging for several independent experiments under each of the three conditions described above were combined and used to generate the bar graphs shown in Fig. 5*E*. As shown, a significant reduction in the height of the NMDA receptor occurred only in the presence of glycine and glutamate (without D($-$)-2-amino-5-phosphonopentanoic acid).
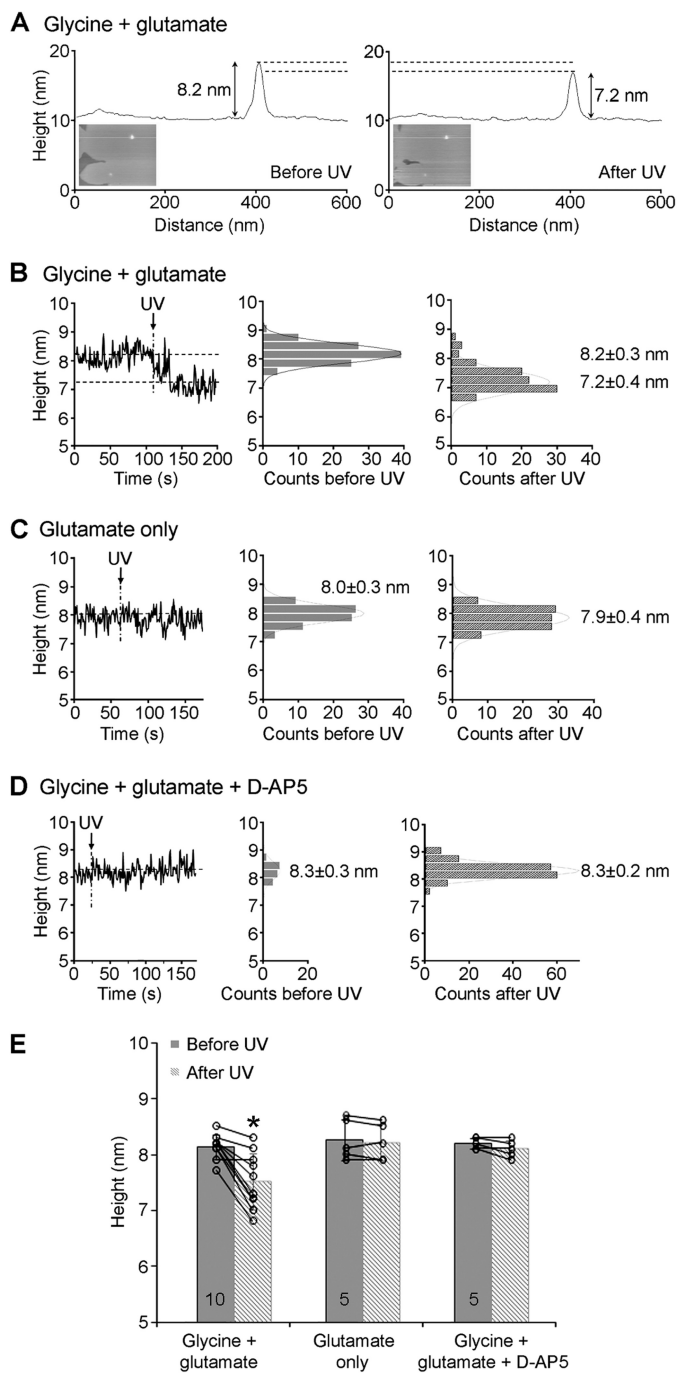
FIGURE 5. **Fast-scan imaging of NMDA receptor height shifts.** *A*, sections through a bilayer-integrated NMDA receptor 7 s apart before and after UV light-induced photolysis of caged glutamate. *B*, changes in receptor height. Frames were captured at 1 Hz. A single receptor was monitored in HEPES-buffered saline containing 1 mM $CaCl_2$, 100 μM glycine, and 100 μM caged glutamate. UV irradiation occurred at 107 s. A fitted Gaussian curve is overlaid on each histogram. The number of frames was 106 before and 92 after irradiation. *C*, effect of omission of glycine. UV irradiation occurred at 72 s. The number of frames was 71 before and 100 after irradiation. *D*, effect of D(−)-2-amino-5-phosphonopentanoic acid (*D-AP5*; 100 μM). UV irradiation occurred at 19 s. The number of frames was 18 before and 151 after irradiation. *E*, bar graphs showing the collected particle heights before and after uncaging for several independent experiments (*numbers* indicated in the *bars*) under the three conditions described above. Pairs of heights before and after UV irradiation for individual experiments are indicated by *connected points*. The *asterisk* indicates a significant change in receptor height following UV irradiation ($p < 0.001$, Student's paired two-tailed t test).

DISCUSSION

Using fast-scan AFM imaging, we have shown that activation results in a rapid structural change in the extracellular region of the GluN1/GluN2A NMDA receptor. Unlike the AMPA receptor, which desensitizes rapidly, the NMDA receptor does not (21, 22); hence, the observed height reduction most likely represents a transition to the activated (*i.e.* open-channel) state.

The height of the extracellular region of the NMDA receptor (~8.6 nm) was considerably smaller than expected from the height of the corresponding region in the crystal structure of the AMPA receptor (~14 nm) (3). Interestingly, AMPA receptors have also been studied using single-particle EM (23–26). The EM structures revealed the expected dimer-of-dimers arrangement, and the various domains of the receptor mentioned above were clearly discernible. Unlike in the crystal structure, however, the NTDs in the EM structures described by Nakagawa and colleagues (24–26) were tilted in one direction, generating an asymmetric structure in which the two dimers had different heights. The EM structure was also shorter than the crystal structure (25). If the arrangement of the two dimers in the NMDA receptor is similar to that in the AMPA receptors, then the individual dimers might again be tilted, accounting for the relatively low profile of the receptor seen here. It should also be kept in mind that the NTDs are likely to arrange differently between NMDA receptors and AMPA/kainate receptors (2). In NMDA receptors, but not AMPA/kainate receptors, the NTDs are known to mediate allosteric signaling, in particular through binding of small ligands acting as allosteric modulators (2, 9, 11, 12, 27). Hence, during allosteric signaling, the NTDs are likely to experience substantial conformational changes.

It has been suggested that agonist binding results in closure of the ABD clamshells, causing them to move apart and downwards toward the membrane (1, 2, 7). Our AFM analysis showed that the predicted reduction in the height of the extracellular region of the receptor upon activation does indeed occur, at least for NMDA receptors. Unfortunately, although AFM is able to determine heights to within a fraction of a nanometer, the measurement of widths is much less accurate because of the tip convolution described above. Furthermore, determination of the width of the receptor will be confounded by the presence of the relatively bulky NTDs above the ABDs. For these reasons, we were unable to discern whether activation caused an increase in the width of the receptor along with the decrease in height.

Fast-scan AFM imaging is perhaps the only technique that permits the visualization of structural changes in proteins at the single-molecule level and under physiological conditions. This method has already yielded detailed information about the operation of proteins as diverse as GroEL (28), the P2X$_4$ receptor for ATP (29), ASIC1a (acid-sensing ion channel 1a) (16), and the Ca^{2+}-ATPase (30). Our present study adds the NMDA receptor to this growing list. We suggest that an extension of our approach might shed significant new light on the structural rearrangements of iGluRs as the receptors pass from the inactive state through the active state and into the desensitized state.

The reduction in the height of the extracellular region of NMDA receptors upon activation may have important implications for the function of the excitatory synapse. iGluRs form large extracellular protrusions that span almost half the width of the synaptic cleft (3). Thus, the extracellular domains (NTDs and ABDs) of iGluRs seem poised to interact with other extracellular and transsynaptic proteins that populate the synapse. NMDA receptors interact directly with the extracellular domains of proteins such as the ephrin B receptor (31, 32) or proteins of the SALM (synaptic adhesion-like molecule) family (33), and these interactions may modulate NMDA receptor activity (34). It is tempting to speculate that a sudden decrease in the height of the extracellular region of the NMDA receptor following its activation will significantly affect the nature and strength of its interactions with its synaptic partners.

REFERENCES

1. Traynelis, S. F., Wollmuth, L. P., McBain, C. J., Menniti, F. S., Vance, K. M., Ogden, K. K., Hansen, K. B., Yuan, H., Myers, S. J., and Dingledine, R. (2010) Glutamate receptor ion channels: structure, regulation, and function. *Pharmacol. Rev.* **62,** 405–496
2. Mayer, M. L. (2011) Emerging models of glutamate receptor ion channel structure and function. *Structure* **19,** 1370–1380
3. Sobolevsky, A. I., Rosconi, M. P., and Gouaux, E. (2009) X-ray structure, symmetry and mechanism of an AMPA-subtype glutamate receptor. *Nature* **462,** 745–756
4. Armstrong, N., and Gouaux, E. (2000) Mechanisms for activation and antagonism of an AMPA-sensitive glutamate receptor: crystal structures of the GluR2 ligand binding core. *Neuron* **28,** 165–181
5. Sun, Y., Olson, R., Horning, M., Armstrong, N., Mayer, M., and Gouaux, E. (2002) Mechanism of glutamate receptor desensitization. *Nature* **417,** 245–253
6. Mony, L., Kew, J. N., Gunthorpe, M. J., and Paoletti, P. (2009) Allosteric modulators of NR2B-containing NMDA receptors: molecular mechanisms and therapeutic potential. *Br. J. Pharmacol.* **157,** 1301–1317
7. Paoletti, P. (2011) Molecular basis of NMDA receptor functional diversity. *Eur. J. Neurosci.* **33,** 1351–1365
8. Furukawa, H., Singh, S. K., Mancusso, R., and Gouaux, E. (2005) Subunit arrangement and function in NMDA receptors. *Nature* **438,** 185–192
9. Gielen, M., Le Goff, A., Stroebel, D., Johnson, J. W., Neyton, J., and Paoletti, P. (2008) Structural rearrangements of NR1/NR2A NMDA receptors during allosteric inhibition. *Neuron* **57,** 80–93
10. Lee, C. H., and Gouaux, E. (2011) Amino-terminal domains of the NMDA receptor are organized as local heterodimers. *PLoS ONE* **6,** e19180
11. Mony, L., Zhu, S., Carvalho, S., and Paoletti, P. (2011) Molecular basis of positive allosteric modulation of GluN2B NMDA receptors by polyamines. *EMBO J.* **30,** 3134–3146
12. Karakas, E., Simorowski, N., and Furukawa, H. (2011) Subunit arrangement and phenylethanolamine binding in GluN1/GluN2B NMDA receptors. *Nature* **475,** 249–253
13. Paoletti, P., Perin-Dureau, F., Fayyazuddin, A., Le Goff, A., Callebaut, I., and Neyton, J. (2000) Molecular organization of a zinc-binding N-terminal modulatory domain in a NMDA receptor subunit. *Neuron* **28,** 911–925
14. Paoletti, P., Ascher, P., and Neyton, J. (1997) High-affinity zinc inhibition of NMDA NR1-NR2A receptors. *J. Neurosci.* **17,** 5711–5725
15. Ando, T., Kodera, N., Takai, E., Maruyama, D., Saito, K., and Toda, A. (2001) A high-speed atomic force microscope for studying biological macromolecules. *Proc. Natl. Acad. Sci. U.S.A.* **98,** 12468–12472
16. Yokokawa, M., Carnally, S. M., Henderson, R. M., Takeyasu, K., and Edwardson, J. M. (2010) Acid-sensing ion channel (ASIC) 1a undergoes a height transition in response to acidification. *FEBS Lett.* **584,** 3107–3110
17. Schneider, S. W., Lärmer, J., Henderson, R. M., and Oberleithner, H. (1998) Molecular weights of individual proteins correlate with molecular volumes measured by atomic force microscopy. *Pflügers Arch.* **435,** 362–367
18. Wenthold, R. J., Prybylowski, K., Standley, S., Sans, N., and Petralia, R. S. (2003) Trafficking of NMDA receptors. *Annu. Rev. Pharmacol. Toxicol.* **43,** 335–358
19. Farina, A. N., Blain, K. Y., Maruo, T., Kwiatkowski, W., Choe, S., and Nakagawa, T. (2011) Separation of domain contacts is required for heterotetrameric assembly of functional NMDA receptors. *J. Neurosci.* **31,** 3565–3579
20. Sprong, H., van der Sluijs, P., and van Meer, G. (2001) How proteins move lipids and lipids move proteins. *Nat. Rev. Mol. Cell Biol.* **2,** 504–513
21. Lester, R. A., and Jahr, C. E. (1992) NMDA channel behavior depends on agonist affinity. *J. Neurosci.* **12,** 635–643
22. Spruston, N., Jonas, P., and Sakmann, B. (1995) Dendritic glutamate receptor channels in rat hippocampal CA3 and CA1 pyramidal neurons. *J. Physiol.* **482,** 325–352
23. Tichelaar, W., Safferling, M., Keinänen, K., Stark, H., and Madden, D. R. (2004) The three-dimensional structure of an ionotropic glutamate receptor reveals a dimer-of-dimers assembly. *J. Mol. Biol.* **344,** 435–442
24. Nakagawa, T., Cheng, Y., Ramm, E., Sheng, M., and Walz, T. (2005) Structure and different conformational states of native AMPA receptor complexes. *Nature* **433,** 545–549
25. Nakagawa, T. (2010) The biochemistry, ultrastructure, and subunit assembly mechanism of AMPA receptors. *Mol. Neurobiol.* **42,** 161–184
26. Shanks, N. F., Maruo, T., Farina, A. N., Ellisman, M. H., and Nakagawa, T. (2010) Contribution of the global subunit structure and stargazin on the maturation of AMPA receptors. *J. Neurosci.* **30,** 2728–2740
27. Gielen, M., Siegler Retchless, B., Mony, L., Johnson, J. W., and Paoletti, P. (2009) Mechanism of differential control of NMDA receptor activity by NR2 subunits. *Nature* **459,** 703–707
28. Yokokawa, M., Wada, C., Ando, T., Sakai, N., Yagi, A., Yoshimura, S. H., and Takeyasu, K. (2006) Fast-scanning atomic force microscopy reveals the ATP/ADP-dependent conformational changes of GroEL. *EMBO J.* **25,** 4567–4576
29. Shinozaki, Y., Sumitomo, K., Tsuda, M., Koizumi, S., Inoue, K., and Torimitsu, K. (2009) Direct observation of ATP-induced conformational changes in single P2X$_4$ receptors. *PLoS Biol.* **7,** e1000103
30. Yokokawa, M., and Takeyasu, K. (2011) Motion of the Ca^{2+}-pump captured. *FEBS J.* **278,** 3025–3031
31. Dalva, M. B., Takasu, M. A., Lin, M. Z., Shamah, S. M., Hu, L., Gale, N. W., and Greenberg, M. E. (2000) EphB receptors interact with NMDA receptors and regulate excitatory synapse formation. *Cell* **103,** 945–956
32. Takasu, M. A., Dalva, M. B., Zigmond, R. E., and Greenberg, M. E. (2002) Modulation of NMDA receptor-dependent calcium influx and gene expression through EphB receptors. *Science* **295,** 491–495
33. Wang, C.-Y., Chang, K., Petralia, R. S., Wang, Y. X., Seabold, G. K., and Wenthold, R. J. (2006) A novel family of adhesion-like molecules that interacts with the NMDA receptor. *J. Neurosci.* **26,** 2174–2183
34. Hansen, K. B., Furukawa, H., and Traynelis, S. F. (2010) Control of assembly and function of glutamate receptors by the amino-terminal domain. *Mol. Pharmacol.* **78,** 535–549